Multiscattering effects in disordered two-dimensional anisotropic Weyl fermions

Zhen Ning [1], Bo Fu,[2,*] Qinwei Shi [3,†] and Xiaoping Wang[1]

[1]*Department of Physics, University of Science and Technology of China, Hefei, Anhui 230026, China*
[2]*Department of Physics, The University of Hong Kong, Pokfulam Road, Hong Kong, China*
[3]*Hefei National Laboratory for Physical Sciences at the Microscale & Synergetic Innovation Center of Quantum Information and Quantum Physics, University of Science and Technology of China, Hefei, Anhui 230026, China*

Exploiting the Lanczos method in momentum space, we determine accurately the quasiparticle properties of disordered two-dimensional Weyl fermions with anisotropic dispersion, which is linear in one direction and quadratic along the other. For comparison, we also present a perturbative analytical analysis based on the Born approximation and renormalization group methods. We reveal that low-energy quasiparticle properties are substantially corrected by multiple impurity scattering processes and manifested by the power-law function of self-energy. Near the nodal point, quasiparticle residue is considerably reduced and vanishes as $Z_E \propto E^r$ with a disorder-dependent exponent r. To highlight the importance of such unconventional quasiparticle residue behavior, we compute the classical diffusive conductivity via the Kubo formalism. We show that the sharp change of Z_E in the vicinity of the nodal point gives rise to the strong temperature dependence of classical conductivity, which can be directly tested by transport measurements in the future.

I. INTRODUCTION

The exploration of the role of disorder is a major activity in condensed matter physics, a subject that has enriched our understanding of many unconventional transport properties such as Anderson localization [1], the integer quantum Hall effect [2], and the anomalous Hall effect [3]. Generally speaking, in a metallic state, the influence of disorder on the quasiparticle and transport properties is characterized by two important physical quantities, i.e., the quasiparticle residue and the elastic scattering time, which can be derived from the self-energy of the Green's function. In the weak scattering limit ($E_F \tau \gg 1$) [4,5], the elastic scattering time can be perturbatively calculated by using the inverse of a dimensionless parameter ($E_F \tau$) as a small expansion parameter. Meanwhile, the influence of disorder on the quasiparticle residue is negligible since the perturbative calculations confirm that the real part of self-energy does not strongly fluctuate with the energy, and thereby quasiparticle residue remains an order of magnitude of unity. However, in the strong scattering limit ($E_F \tau \lesssim 1$), it is usually believed that multiple scattering processes involving many impurity centers have driven most conventional disordered metals into insulator states—such a phenomenon is called Anderson localization. As Anderson localization occurs in this new regime, all states are localized, thus the quasiparticle residue and the elastic scattering time lose their real meanings to describe the effect of disorder on the hopping transport at finite temperatures.

Because of the divergence of the wavelength at the nodes of semimetals [6,7], as exemplified by graphene, the effects of disorder are drastically different from those in conventional metals with a finite Fermi surface—those Dirac fermion systems easily enter into the strong scattering limit as the Fermi energy is close to the nodes [8]. Therefore, it is naturally expected that the interference effect, originating from many impurities being multiply scattered, will dominate physics around the nodal point; these processes are different from the usual weak localization effect. Indeed, previous perturbative calculations show that such multiple impurity scattering processes not only have a considerable influence on the elastic scattering time [9,10] but also give rise to the ultraviolet logarithmic corrections to the quasiparticle residue [11,12].

Similarly, it is anticipated that multiple impurity scattering events may also play an important role in two-dimensional (2D) anisotropic Weyl fermions (AWFs) [13–19], the gapless low-energy quasiparticles with anisotropic dispersion emerging from the merging point of two Dirac nodes in the Brillouin zone [20–22]. The possible physical realization of this anisotropic dispersion has already been reported in previous studies [23–27]. Indeed, the first-order Born approximation shows that quasiparticle residue vanishes at the nodal point as $Z_E \propto (E)^{-1/2}$; in addition, the self-consistent Born approximation predicts Z_E approaches a finite constant, $Z_{E\to0} = 1/2$ [28]. On the other hand, a renormalization group (RG) analysis [17] on the tree level shows that disorder is a relevant perturbation in the AWF system, in contrast with its isotropic partner such as graphene, where the disorder is marginally relevant. A further analysis based on one-loop RG in this work confirms that quasiparticle residue vanishes at a special energy scale (E_c) near the nodal point, $Z_E \propto \sqrt{1 - (E_c/E)^{1/2}}$ [28], below which RG does not work. For

*Corresponding author: fubo@hku.hk
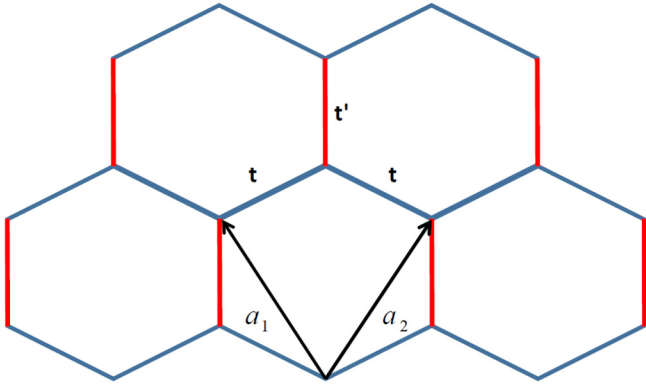†Corresponding author: phsqw@ustc.edu.cn

FIG. 1. Lattice structure of deformed graphene with anisotropic hopping integrals t, t'. The nearest-neighbor lattice vectors are $\vec{a}_1$, $\vec{a}_2$, discussed in the text.

comparison, the quasiparticle residue in graphene goes to zero as $Z_E \propto \sqrt{\ln(E/E_c)}$ [11,12]. Those three approximative approaches unveil parts of the properties of quasiparticle residue, reflecting the importance of multiple impurity scattering processes, however, they present inconsistent results. To uncover the physics near the nodal point, a more careful nonperturbative analysis involving all multiscattering events is needed.

In this paper, we present exact numerical results of the quasiparticle properties in disordered AWFs by using the Lanczos method that is able to rigorously treat all multiscattering events. Our simulation clearly reveals that the self-energy obeys a common power-law behavior, whose exponent is dependent on the disorder strength. This nonanalytic correction serves as the very basis for the unusual behaviors of quasiparticles and many other physical properties surrounding the nodal point. We also show that quasiparticle residue goes to zero as $Z_E \propto E^r$ in the vicinity of the nodal point. This unconventional behavior is distinctly different from that predicted by the Born approximation and one-loop RG calculations [28]. Furthermore, we show that such quasiparticle behavior gives rise to the strong temperature dependence of classical diffusive conductivity along the linear dispersion direction.

II. MODEL AND METHOD

In order to study the effects of disorder on anisotropic Weyl fermions numerically, we choose the deformed honeycomb lattice for simplicity [24]. In the absence of disorder, a tight-binding model of the Hamiltonian is $H_0 = \sum_{\langle ij \rangle} t_{ij} |i\rangle \langle j| +$ H.c., where t_{ij} is the hopping energies t, t' (see Fig. 1). The Hamiltonian in **k** space is

$$H = \begin{pmatrix} 0 & f(k) \\ f^*(k) & 0 \end{pmatrix}, \tag{1}$$

with the function $f(k)$ defined as $f(k) = t' + t e^{i\vec{k} \cdot \vec{a}_1} + t e^{i\vec{k} \cdot \vec{a}_2}$, where $\vec{a}_1 = a(\frac{\sqrt{3}}{2}, \frac{3}{2})$, $\vec{a}_2 = a(-\frac{\sqrt{3}}{2}, \frac{3}{2})$ are elementary vectors of the Bravais lattice, and a is the distance between atoms and is set to $a = 1$. When $t' = t$, the Hamiltonian is the usual model of graphene with two Dirac nodes at $K = (\frac{2\pi}{3\sqrt{3}a}, \frac{2\pi}{3a})$, $K' = (-\frac{2\pi}{3\sqrt{3}a}, \frac{2\pi}{3a})$ in the Brillouin zone. More interestingly, by setting $t' = 2t$, the two Dirac nodes merge into a single

point at $D = (0, \frac{2\pi}{3a})$ to form anisotropic Weyl fermions. The low-energy effective continuum model can be written as [24]

$$H = c_x k_x^2 \sigma_x + c_y k_y \sigma_y, \tag{2}$$

with parameters $c_x = \frac{3}{4} t a^2$, $c_y = 3ta$, where $1/(2c_x) = m$ is the effective mass along the x direction and c_y is the velocity along the y direction, and the quasiparticle dispersion is $\epsilon_{k\pm} = \pm\sqrt{(c_x k_x^2)^2 + (c_y k_y)^2}$. Thus, the low-energy quasiparticle exhibits a unique anisotropic dispersion which is linear in one direction and quadratic along the other.

To explore the disorder effect, the sublattice uncorrelated Anderson-type disorder is introduced by the on-site random potential distributed independently within $[-W/2, W/2]$. A dimensionless parameter $\gamma = \frac{A_c W^2}{12\pi \sqrt{t} \sqrt{c_x c_y}} r_\phi$ is used to characterize the strength of disorder obtained from Fermi's golden rule as usual. Here, $A_c = \frac{3\sqrt{3}}{2} a^2$ is the area of the unit cell, and the constant $r_\phi = \frac{1}{\pi} \int \frac{d\phi}{\sqrt{\cos\phi}} \approx 0.835$. The energy is measured in units of $t = 1$ and we set $\hbar = 1$ in this work. In order to suppress the artificial finite-size effect, we choose a large sample $L^2 = (10^4)^2$ and calculate its retarded self-energy in the quasiparticle representation $\Sigma(E, \mathbf{k})$ by the momentum-space Lanczos recursive method [29–31]. A small artificial damping parameter 10^{-3} is used in our simulation so that we can extract the self-energy of the single-particle Green's function with a high-energy resolution. In our simulation, we find that both real and imaginary parts of the self-energy are insensitive to wave vector **k** [30], are independent of the band index [32], and are dependent only on the energy E.

III. SELF-ENERGY AND QUASIPARTICLE PROPERTIES

The imaginary part of the self-energy Im $\Sigma(E)$ for disordered 2D AWFs with different strengths of disorder γ is plotted in Fig. 2(a). Notice that the first-order Born approximation predicts the square-root behavior $\sqrt{E}$ [28] of the self-energy. However, as shown in Fig. 2(a), the self-energy has distinct structures as the disorder strength increases; a natural generalization can be made by observing that Im $\Sigma(E)$ gradually deviates from the square-root behavior and the value of the imaginary part of self-energy at zero energy Σ_0 is increased. These characterized features inspire us to use a power-law formula to fit our numerical results,

$$\text{Im } \Sigma(E) = -\Sigma_0 - \Delta |E|^{\frac{1}{2} + \beta}. \tag{3}$$

In order to further corroborate that the imaginary part of self-energy can be described by a constant plus power-law function, we plot the imaginary part of the self-energy on a log-log scale within an energy window $E \in [0.01, 0.2]$. As shown in Fig. 3, the power-law form of the self-energy provides a fairly good fit in this energy regime.

Here, we report the fitting results of the power-law self-energy Im $\Sigma(E)$ in the weak disorder strength. The fitting parameters β, Δ, and Σ_0 as a function of disorder strength γ are shown in Figs. 4(a)–(c), respectively. The fitting parameters β and Δ are approximately proportional to the disorder strength as $\beta = 11.3\gamma$ and $\Delta = 2.1\gamma$. The dependence of β on γ clearly reflects that proper treatment of all orders of multiscattering events will fundamentally modify
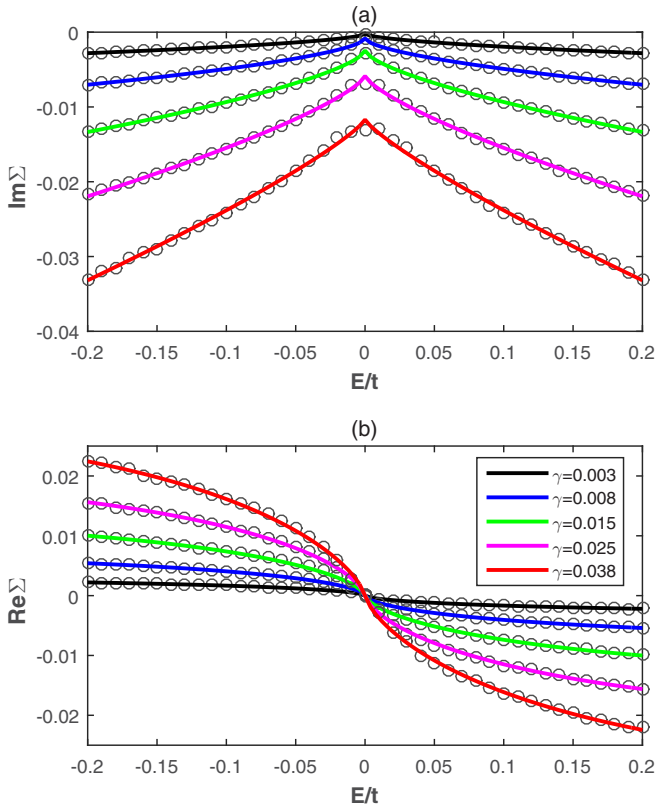
FIG. 2. (a) Imaginary and (b) real parts of the self-energy of disordered 2D AWFs as a function of energy E with different disorder strengths γ. The open circles are the numerical results while the solid lines are the fitting curves of Eqs. (3) and (5), respectively.
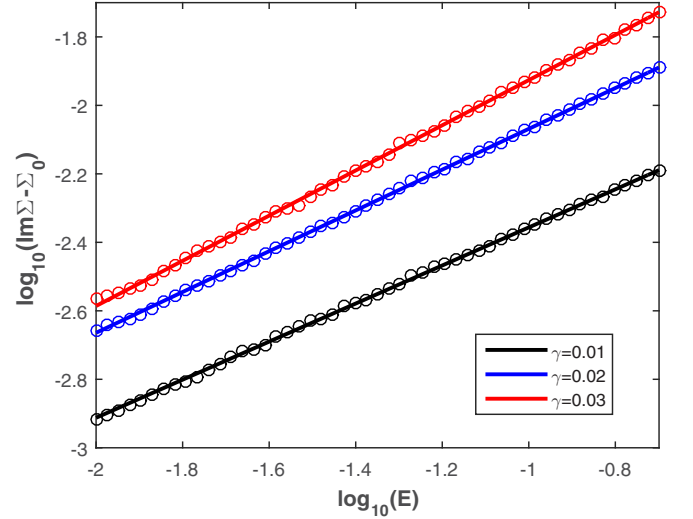

FIG. 3. The logarithmic plot shows constant plus power-law behavior of the imaginary part of self-energy on different strengths of disorder; the circles are numerical results and the solid line is the linear fitting over an energy scale $E \in [0.01, 0.2]$ (or $\log_{10} E = [-2, -0.7]$).

the quasiparticle properties of AWF, which is out of reach of conventional perturbation theory. More intriguingly, with the help of the one-loop RG approach (see Ref. [28] for a detailed derivation), we find an expression, Eq. (4), to fit Σ_0 as a function of disorder strength, interpreted as a characteristic low-energy scale E_c, and the system enters into the strong-coupling regime below the characteristic energy E_c [12]. The calculation of the RG [28] shows that the characteristic energy E_c is written as

$$E_c = \frac{g_1 \gamma^2}{(1 + g_2 \gamma)^2}. \quad (4)$$

The constants g_1, g_2 can be obtained by fitting the numerical data of Σ_0 with $g_1 \approx 10.7$, $g_2 \approx 4.3$. Notice that a similar relationship between the Σ_0 and the E_c has been reported in disordered graphene [11,12]. As shown in Fig. 2(a), the agreement between Eq. (3) and the numerical results is excellent.

Moreover, the corresponding fitting formula for the real part of self-energy $\text{Re}\,\Sigma(E)$ can be constructed via the Kramers-Kronig relation [33],

$$\text{Re}\,\Sigma(E) = D\,\text{sgn}(E)|E|^{\frac{1}{2}+\beta} + CE, \quad (5)$$

where sgn denotes the signum function, and the parameters are $D = -\tan[\frac{\pi}{2}(\frac{1}{2}+\beta)]\Delta$, and $C = -\frac{2\Delta E_c^{\beta-\frac{1}{2}}}{\pi(\beta-\frac{1}{2})}$ [34]. The comparison between the fitting formula and numerical results of $\text{Re}\,\Sigma(E)$ is shown in Fig. 2(b), again in very

good agreement with each other. Now, we can easily extract the quasiparticle residue via the formula $Z_E = 1/[1 - \partial_E \text{Re}\,\Sigma(E)]$. Near the nodal point, Z_E scales as $E^{\frac{1}{2}-\beta}$. Equations (3) and (5) are the central findings of our work.

We then study multiscattering effects on several fundamental physical quantities such as the elastic mean free time (τ), group velocity (v_g), and mean free path (l). As the Fermi energy approaches the nodal point, the self-energy function $\text{Im}\,\Sigma(E)$ approaches a constant Σ_0 and the decay time $\tau = 1/[2Z_E|\text{Im}\,\Sigma(E)|]$ [35] is divergent as $\propto E^{-\frac{1}{2}+\beta}$. The group velocity along the direction of linear dispersion is renormalized by a factor of Z_E as $v_g = Z_E c_y$, which is reduced quickly down to zero as $v_g \propto E^{\frac{1}{2}-\beta}$, as we can see in Fig. 5(a). For comparison, we plot the prediction based on the one-loop RG theory $Z_E \propto \sqrt{1 - (E_c/E)^{1/2}}$ and our simulation result in Fig. 5(b) for the same disorder strength. The two curves
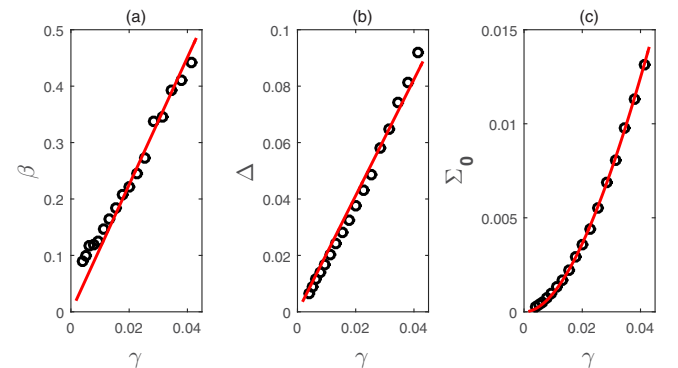

FIG. 4. The fitting parameters of self-energy β, Δ, and Σ_0 as functions of the disorder strength γ are shown in (a)–(c), respectively. The black open circles are the numerical results, and red solid lines are fitting curves.
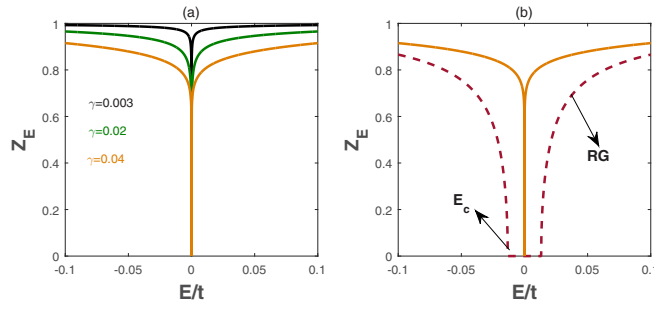
FIG. 5. (a) Quasiparticle residue Z_E as a function of energy E for different strengths of disorder. (b) Comparison between the RG results of Z_E with the curve ($\gamma = 0.04$) in the left panel.

are close to each other in $E/E_c \gg 1$ and behave differently as $E \to E_c$, below which the one-loop RG breaks down. The mean free path along the direction of linear dispersion $l_y = v_g \tau = c_y/[2|\mathrm{Im}\,\Sigma(E)|]$ is independent of Z_E and approaches a constant $1/\Sigma_0$ as $E \to 0$. The one-loop RG calculation can obtain the same mean free path at $E = E_c$, but beyond this length scale, the renormalization process should be stopped.

IV. TRANSPORT BEHAVIOR

The finding of the accurate self-energy Eqs. (3) and (5) can also lead to further studies of the diffusive transport behavior [13–16] of AWF. Based on the standard Kubo-Greenwood formula [36], the longitudinal conductivity $\sigma_{\mu\mu}(\mu = x, y)$ can be expressed as

$$\sigma_{\mu\mu}(E_F, T) = \int d\omega \left(-\frac{\partial f(\omega, E_F)}{\partial \omega}\right) K_{\mu\mu}(\omega),$$

$$K_{\mu\mu}(\omega) = \frac{e^2}{\pi} \int \frac{d^2k}{(2\pi)^2} \mathrm{Tr}[\hat{v}_\mu \hat{A}(k, \omega) \hat{v}_\mu \hat{A}(k, \omega)], \quad (6)$$

where $f(\omega) = 1/(e^{(\omega - E_F)/(k_B T)} + 1)$ is the Fermi-Dirac distribution function, E_F is the Fermi energy, and $\hat{A}$ is the spectral function containing the accurate self-energy discussed in this work. In the following discussion, for simplicity, we define two constants $\sigma_{xx}^0 = \frac{e^2}{\pi} \frac{\sqrt{c_x}\sqrt{t}}{\pi^2 c_y}$ and $\sigma_{yy}^0 = \frac{e^2}{\pi} \frac{c_y}{4\pi^2 \sqrt{c_x}\sqrt{t}}$ as the unit of conductivity along the direction of quadratic and linear dispersion [28], respectively. We depict the zero-temperature conductivity as a function of Fermi energy E_F in Figs. 6(a) and 6(b). In this case, the function $-\frac{\partial f(\omega, E_F)}{\partial \omega}$ in Eq. (6) is replaced by the delta function $-\delta(\omega - E_F)$. The residual conductivity $\sigma_{\mu\mu}^r$ at the nodal point $E_F = 0$ is directly dependent on the strength of disorder and behaves as $\sigma_{xx}^r \propto \sqrt{\Sigma_0}$, $\sigma_{yy}^r \propto 1/\sqrt{\Sigma_0}$, respectively. Our results are in contrast to the prediction obtained by the Boltzmann transport theory such as $\sigma_{xx} \propto \frac{E_F}{\gamma} = 0$ and $\sigma_{yy} \propto \frac{1}{\gamma}$ [13–15].

As the Fermi energy is away from the nodal point, our results qualitatively agree with the calculation from Boltzmann transport theory. The $\sigma_{xx}(E_F)$ increases linearly with the Fermi energy [see Fig. 6(a)] which exhibits the conventional behavior of 2D Schrödinger electron gas. The conductivity σ_{xx} is proportional to the Fermi energy and the inverse of disorder strength $\sigma_{xx} \propto \frac{E_F}{\gamma}$. Therefore, as shown in Figs. 6(c) and 6(e), our results of the conductivity σ_{xx} at finite temperature can
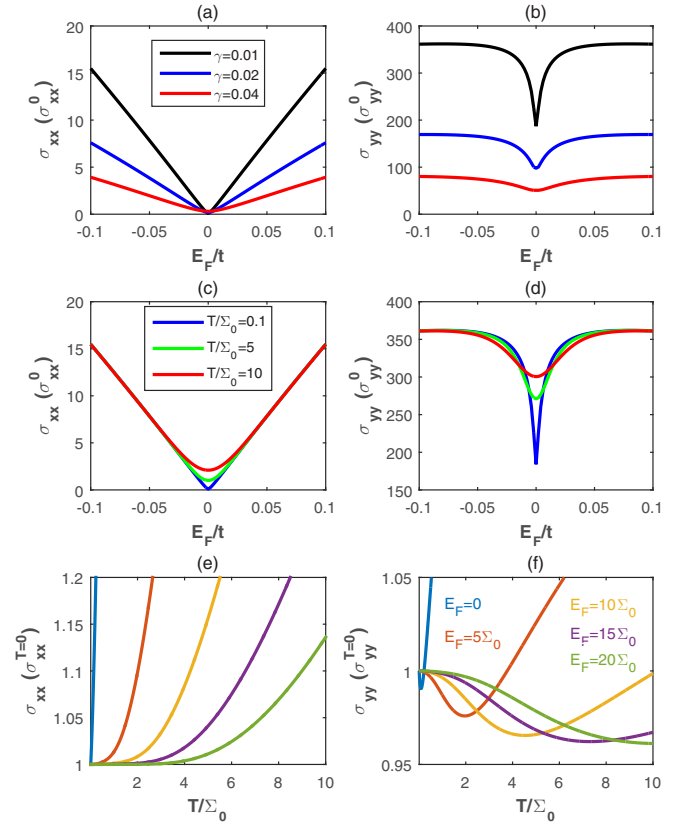

FIG. 6. Zero-temperature conductivity along the (a) x direction σ_{xx} and (b) y direction σ_{yy} for different disorder strengths. (c) and (d) show the finite-temperature effect on conductivity $\sigma_{\mu\mu}(E_F)$ for different temperatures. (e) and (f) show the temperature dependence of the conductivity $\sigma_{\mu\mu}(T)$ for different Fermi energies, where they are measured by their value at zero temperature $\sigma_{xx}^{T=0}$, $\sigma_{yy}^{T=0}$. In (c)–(f), the strength of disorder is fixed at $\gamma = 0.01$, which corresponds to an energy scale $\Sigma_0 \approx 10^{-3}t$.

also be well described by the Boltzmann transport theory, signifying that multiple scattering effects on this direction are very weak and hardly tested by transport measurements. However, as the strength of disorder increases, there still exists a distinct quantitative difference between our results and the Boltzmann's prediction [28], reflecting the importance of multiscattering effects around the nodal point.

However, multiscattering events can significantly affect the conductivity along the k_y direction as plotted in Figs. 6(b), 6(d) and 6(f). At zero temperature, in the presence of weak disorder strength ($\gamma = 0.01$), the conductivity σ_{yy} displays a sharp dip around the nodal point due to the multiscattering effect. As the disorder strength increases, such a dip is gradually smeared. Therefore, at weak disorder, the dip can be manifested by its strong temperature dependence as shown in Fig. 6(d). Moreover, as shown in Fig. 6(f), we plot the conductivity σ_{yy} as a function of temperature for several different Fermi energies varying from $E_F = 0$ to 0.02. At a high Fermi energy (corresponding to a high carrier density), the conductivity σ_{yy} exhibits metallic temperature behavior ($d\sigma/dT < 0$). However, in the low doping regime, if the temperature is not too small, it shows an insulating-type temperature dependence ($d\sigma/dT > 0$). Therefore, the

conductivity $\sigma_{yy}(T)$ shows a nonmonotonic temperature dependence in Fig. 6(f), and there exists a local minimum at finite temperature. Due to smearing of the dip of conductivity $\sigma_{yy}(E_F)$ at a moderate disorder strength $\gamma = 0.04$, as shown in Fig. 6(b), the conductivity is approximately independent of Fermi energy, and it is thereby independent of temperature. In this scenario, although the qualitative behavior of conductivity is consistent with the prediction of Boltzmann's theory, the quantitative behavior is still quite different. Thus, the strong temperature dependence of conductivity can be tested in the ultrahigh-mobility AWF sample along the direction of relativistic quasiparticle dispersion.

V. DISCUSSIONS

Up to now, we have focused on studying nontrivial quasiparticle behavior and classical diffusive conductivity near the nodal point (including the contribution from the ladder vertex correction [28]), and neglect the contribution from the weak localization correction. In fact, the previous calculation of the weak (or antiweak) localization correction to the conductivity only works well in the weak scattering limit. In this weak scattering limit, our calculation [28] finds that the weak localization correction to the conductivity obeys the conventional formula $\sigma_{\text{wl}} \propto -\ln\left(\frac{L_{\text{IR}}}{l_e}\right)$ [1], where $l_e = v_F \tau$ is the electron mean free path and L_{IR} is the infrared cutoff, confirming that the quantum correction to the conductivity depends sensitively on the symmetry of the system. Notice that our discussed system belongs to the orthogonal class. However, as the energy approaches the nodal point, our discussed system naturally enters into the strong scattering limit. In this situation, how to treat the contribution to the conductivity from the quantum interference process is still a challenging task and deserves further study. More importantly, comparing our results with real experiments may uncover some useful information about the correction from the quantum interference process in this strong scattering limit.

In this work, notice that we have focused on studying the effects of the sublattice uncorrelated Anderson disorder on the quasiparticle properties. Generally speaking, because of the divergence of the wavelength near the nodal point, it is expected that correlated and uncorrelated disorder may give rise to similar physical results. However, in this anisotropic system, the situation is quite different. It is reported [14,17] that sublattice correlated Anderson disorder may generate a mass term in the effective Hamiltonian of AWF, which leads to a quantum phase transition from a semimetal to a gapped insulator. It is very interesting and important to investigate the role of multiple impurity scattering processes in this kind of quantum phase transition. We will defer consideration of this important issue to future works.

In summary, using the momentum-space Lanczos method, we have investigated multiple scattering effects on the quasiparticle and transport properties of disordered anisotropic Weyl fermions. A power-law behavior of the self-energy is constructed for describing the nontrivial quasiparticle properties which lead to unconventional transport behavior and can be directly related to experimental observations.

[1] P. A. Lee and T. V. Ramakrishnan, Rev. Mod. Phys. **57**, 287 (1985).

[2] A. W. W. Ludwig, M. P. A. Fisher, R. Shankar, and G. Grinstein, Phys. Rev. B **50**, 7526 (1994).

[3] N. Nagaosa, J. Sinova, S. Onoda, A. H. MacDonald, and N. P. Ong, Rev. Mod. Phys. **82**, 1539 (2010).

[4] A. F. Ioffe and A. R. Regel, Prog. Semicond. **4**, 237 (1960).

[5] Y. Imry, *Introduction to Mesoscopic Physics* (Oxford University Press, Oxford, UK, 2002).

[6] A. H. Castro Neto, F. Guinea, N. M. R. Peres, K. S. Novoselov, and A. K. Geim, Rev. Mod. Phys. **81**, 109 (2009).

[7] A. V. Balatsky, I. Vekhter, and J. X. Zhu, Rev. Mod. Phys. **78**, 373 (2006).

[8] A. Altland, Phys. Rev. Lett. **97**, 236802 (2006).

[9] A. A. Nersesyan, A. M. Tsvelik, and F. Wenger, Phys. Rev. Lett. **72**, 2628 (1994).

[10] A. A. Nersesyan, A. M. Tsvelik, and F. Wenger, Nucl. Phys. B **438**, 561 (1995).

[11] I. L. Aleiner and K. B. Efetov, Phys. Rev. Lett. **97**, 236801 (2006).

[12] P. M. Ostrovsky, I. V. Gornyi, and A. D. Mirlin, Phys. Rev. B **74**, 235443 (2006).

[13] S. Banerjee and W. E. Pickett, Phys. Rev. B **86**, 075124 (2012).

[14] P. Adroguer, D. Carpentier, G. Montambaux, and E. Orignac, Phys. Rev. B **93**, 125113 (2016).

[15] P. Nualpijit, A. Sinner, and K. Ziegler, Phys. Rev. B **97**, 235411 (2018).

[16] J. P. Carbotte, K. R. Bryenton, and E. J. Nicol, Phys. Rev. B **99**, 115406 (2019).

[17] D. Carpentier, A. A. Fedorenko, and E. Orignac, Europhys. Lett. **102**, 67010 (2013).

[18] P. L. Zhao, J. R. Wang, A. M. Wang, and G. Z. Liu, Phys. Rev. B **94**, 195114 (2016).

[19] H. Isobe, B. J. Yang, A. Chubukov, J. Schmalian, and N. Nagaosa, Phys. Rev. Lett. **116**, 076803 (2016).

[20] L. K. Lim, J.-N. Fuchs, and G. Montambaux, Phys. Rev. Lett. **108**, 175303 (2012).

[21] M. Bellec, U. Kuhl, G. Montambaux, and F. Mortessagne, Phys. Rev. Lett. **110**, 033902 (2013).

[22] B. J. Yang, E. G. Moon, H. Isobe, and N. Nagaosa, Nat. Phys. **10**, 774 (2014).

[23] S. Banerjee, R. R. P. Singh, V. Pardo, and W. E. Pickett, Phys. Rev. Lett. **103**, 016402 (2009).

[24] P. Dietl, F. Piechon, and G. Montambaux, Phys. Rev. Lett. **100**, 236405 (2008).

[25] M. O. Goerbig, J.-N. Fuchs, G. Montambaux, and F. Piechon, Phys. Rev. B **78**, 045415 (2008).

[26] L. Tarruell, D. Greif, T. Uehlinger, G. Jotzu, and T. Esslinger, Nature (London) **483**, 302 (2012).

[27] J. Kim, S. S. Baik, S. H. Ryu, Y. Sohn, S. Park, B.-G. Park, J. Denlinger, Y. Yi, H. J. Choi, and K. S. Kim, Science **349**, 723 (2015).

[28] See Supplemental Material at http://link.aps.org/supplemental/10.1103/PhysRevB.102.134207 for the detailed derivation and renormalization group analysis.

[29] B. Fu, W. Zhu, Q. W. Shi, Q. X. Li, J. L. Yang, and Z. Y. Zhang, Phys. Rev. Lett. **118**, 146401 (2017).

[30] W. Zhu, Q. W. Shi, X. R. Wang, X. P. Wang, J. L. Yang, J. Chen, and J. G. Hou, Phys. Rev. B **82**, 153405 (2010).

[31] S. D. Wu, L. Jing, Q. X. Li, Q. W. Shi, J. Chen, H. B. Su, X. P. Wang, and J. L. Yang, Phys. Rev. B **77**, 195411 (2008).

[32] One analytical evidence is from the calculation of the matrix element of self-energy under the quasiparticle eigenfunctions $|k, s\rangle$ (see Ref. [28] for details), $\Sigma_{ks,k's'}(E) = \overline{\langle k, s|\hat{V}\hat{G}(E)\hat{V}|k', s'\rangle} = \Sigma(E)\delta_{kk'}\delta_{ss'}$.

[33] The general Kramers-Kronig relationship is $\text{Re}\,\Sigma(\omega) = \frac{1}{\pi}\text{P}\int d\omega' \frac{\text{Im}\,\Sigma(\omega')}{\omega'-\omega}$, where P signifies the Cauchy principal value of the integral.

[34] We note that there is no singularity as $b \to 1$, because if we set $h = 1 - b$ and $D = -\tan[\frac{\pi}{2}(1-h)]\Delta \underset{h\to 0}{=} \frac{-2\Delta}{\pi h}$, then, the limit of $\text{Re}\,\Sigma(E)$ becomes $\frac{-2\Delta}{\pi}E\lim_{h\to 0}u_c^{-h}\frac{(u_c/|E|)^h-1}{h} = \frac{-2\Delta}{\pi}E\ln(\frac{u_c}{|E|})$.

[35] G. D. Mahan, *Many Particle Physics* (Kluwer Academic/Plenum, New York, 2000).

[36] E. Akkermans and G. Montambaux, *Mesoscopic Physics of Electrons and Photons* (Cambridge University Press, Cambridge, UK, 2007).